Article

SOURCE DATA | TRANSPARENT PROCESS

EMBO reports

Protein phosphatase PP2A regulates microtubule orientation and dendrite pruning in *Drosophila*

Menglong Rui[1,†], Kay Siong Ng[1,†], Quan Tang[1,2], Shufeng Bu[1,2] & Fengwei Yu[1,2,3,4,*]

Abstract

Pruning that selectively eliminates inappropriate projections is crucial for sculpting neural circuits during development. During *Drosophila* metamorphosis, ddaC sensory neurons undergo dendrite-specific pruning in response to the steroid hormone ecdysone. However, the understanding of the molecular mechanisms underlying dendrite pruning remains incomplete. Here, we show that protein phosphatase 2A (PP2A) is required for dendrite pruning. The catalytic (Microtubule star/Mts), scaffolding (PP2A-29B), and two regulatory subunits (Widerborst/Wdb and Twins/Tws) play important roles in dendrite pruning. Functional analyses indicate that PP2A, via Wdb, facilitates the expression of Sox14 and Mical prior to dendrite pruning. Furthermore, PP2A, via Tws, governs the minus-end-out orientation of microtubules (MTs) in the dendrites. Moreover, the levels of Klp10A, a MT depolymerase, increase when PP2A is compromised. Attenuation of Klp10A fully rescues the MT orientation defects in *mts* or *pp2a-29b* RNAi ddaC neurons, suggesting that PP2A governs dendritic MT orientation by suppressing Klp10A levels and/or function. Taken together, this study sheds light on a novel function of PP2A in regulating dendrite pruning and dendritic MT polarity in sensory neurons.

Keywords dendrite pruning; Klp10A; microtubule orientation; neuron; protein phosphatase

Subject Categories Cell Adhesion, Polarity & Cytoskeleton; Neuroscience; Post-translational Modifications & Proteolysis

DOI 10.15252/embr.201948843 | Received 12 July 2019 | Revised 20 February 2020 | Accepted 4 March 2020 | Published online 18 March 2020

EMBO Reports (2020) 21: e48843

Introduction

Neuronal pruning that precisely removes exuberant neuronal connections and excessive neurites is essential for the maturation of the nervous system during animal development [1]. Neuronal pruning is a highly conserved process widely occurring in both vertebrates and invertebrates during the development of the nervous systems [2,3]. In both central and peripheral nervous systems of mammals, neurons selectively eliminate the superfluous and unneeded neurites to establish functional circuits [4]. *Drosophila* has emerged as an attractive model to elucidate the underlying mechanisms of neuronal pruning over the last decade [5,6]. In *Drosophila,* the nervous system undergoes dramatic remodeling during metamorphosis in order to build up adult-specific neuronal networks [3,7]. In the central nervous system (CNS), mushroom body γ neurons remove their axonal branches from the dorsal and medial lobes as well as their entire dendrites and subsequently regrow to form adult-specific circuits [8]. Likewise, in the peripheral nervous system (PNS), some sensory neurons, including dorsal dendritic arborization (da) neurons, undergo either apoptosis or pruning during early metamorphosis. Class I (ddaD/E) and class IV (ddaC, also known as C4da) neurons selectively remove their larval dendrite branches but keep their axons intact [9,10], while class II (ddaB) and class III (ddaA/F) neurons are apoptotic [10]. Defects in neuronal pruning have been shown to be associated with brain disorders, such as autism spectrum disorder (ASD) and schizophrenia [11,12]. Thus, studying the molecular and cellular mechanisms of developmental pruning would potentially contribute to our understanding of the pathogenesis of human brain disorders.

Drosophila ddaC sensory neuron is an excellent model to study developmental dendrite pruning due to its highly branched dendrites and the ease of live-cell imaging. In response to a late-larval pulse of the steroid molting hormone 20-hydroxyecdysone (20E), ddaC neurons undergo a stereotyped pruning process in which their larval dendrites are first severed at the proximal regions, subsequently fragmented and removed by phagocyte-mediated debris clearance (Fig 1A) [9,10,13]. Dendrite pruning of ddaC neurons is initiated by an ecdysone-induced signaling cascade. The neuron-specific ecdysone receptor EcR-B1, which is upregulated in response to the late-larval ecdysone pulse, is required to induce the expression of the transcription factor Sox14. Sox14 in turn upregulates the expression of the cytoskeletal regulator Mical [14]. Other molecules and signal pathways including ubiquitin–proteasome system [15,16], Ik2/Kat60L [17,18], caspases [15,19], headcase [20], microtubule (MT) regulators/motors [21–23], calcium signaling [24], insulin pathway [16], endocytosis [25–27], and the JNK

1 Temasek Life Sciences Laboratory, National University of Singapore, Singapore City, Singapore
2 Department of Biological Sciences, National University of Singapore, Singapore City, Singapore
3 NUS Graduate School for Integrative Sciences and Engineering, Centre for Life Sciences, Singapore City, Singapore
4 Neuroscience and Behavioral Disorder Program, Duke-NUS Medical School Singapore, Singapore City, Singapore
*Corresponding author. Tel: +65 6872 7475; E-mail: fengwei@tll.org.sg
†These authors contributed equally to the work

signaling pathway [28] have been documented to regulate dendrite pruning of ddaC neurons. It has been recently reported that PAR-1 and Patronin play important roles in regulating MT stability and orientation during dendrite pruning [22,23,29]. However, our understanding of the molecular and cellular mechanisms underlying dendrite pruning is still far from complete.

In a genome-wide RNA interference (RNAi) screen, we isolated Microtubule star (Mts), a catalytic subunit of protein phosphatase 2A (PP2A), which is required for dendrite pruning of ddaC neurons. PP2A is a highly conserved and ubiquitous serine–threonine phosphatase [30,31]. In mammals, the core enzyme exists as a dimer ($PP2A_D$) consisting of a catalytic C subunit ($PP2A_C$) and a scaffolding A subunit of 65 kDa (PR65). A regulatory B subunit is associated with this core architecture to form the holoenzyme [30]. Several isoforms of A (α and β), C (α and β), and B (B, B′, B″, and B ‴) subunits have been found to be encoded by distinct genes or alternative splicing of a single gene [30] (Appendix Fig S1A). PP2A is involved in many essential cellular functions including cell cycle progression, cellular metabolism, migration, and apoptosis [32–34]. In *Drosophila,* heterotrimeric PP2A holoenzyme comprises the A subunit PP2A-29B, the C subunit Mts, and one of the following regulatory B subunits, including Twins (Tws, B subunit), Well-rounded (Wrd, B′ subunit), Widerborst (Wdb, B″ subunit), and PR72 (B‴ subunit) [31]. PP2A regulates various developmental processes, including tissue pattern [35], planar cell polarity [36], asymmetric cell division [37,38], and synapse formation [39]. PP2A has been reported to regulate MT cytoskeletal organization in both mitotic and postmitotic cells [39,40].

In this study, we report an important role of PP2A in dendrite pruning of sensory neurons. We show that PP2A, via its regulatory subunit Wdb, regulates dendrite pruning by activating the expression of Sox14 and Mical. Interestingly, PP2A, via another regulatory subunit Tws, is responsible for the uniform MT orientation in dendrites. Thus, our study reveals, for the first time, that the protein phosphatase PP2A regulates dendrite pruning and dendritic MT polarity via ecdysone signaling and a MT-depolymerizing kinesin, respectively.

Results

The catalytic subunit of PP2A Mts is required for ddaC dendrite pruning

To identify novel players of dendrite pruning, we previously conducted an unbiased genome-wide RNAi screen in ddaC neurons [14]. In this screen, we isolated *mts* which is required for dendrite pruning. The neurons expressing the control RNAi construct completely eliminated larval dendrites at 16 h APF (Fig 1B, I and J). In contrast, knockdown of *mts*, via two independent RNAi transgenes (#1, BSC27723 and #2, v41924), led to consistent dendrite pruning defects in the vast majority of ddaC neurons at the same time point (85 and 97%, respectively) (Fig 1C, I and J, Appendix Fig S1B). *mts* encodes the catalytic subunit of PP2A which was shown to localize as star-like structures on mitotic spindles in dividing cells [40]. To further verify the role of *mts* in ddaC dendrite pruning, we next generated mutant clones using the strong hypomorphic allele mts^{299} [38] and the null allele mts^{xe2258} [41]. Consistently, in contrast to no pruning defects in the control clones (Fig 1D, I and J), we observed similar severing defects in 78 and 100% of mts^{299} and mts^{xe2258} ddaC clones, respectively (Figs 1E, I and J, and EV1A). The pruning phenotypes associated with mts^{299} and mts^{xe2258} mutants were fully rescued by the expression of the wild-type Mts protein (Figs 1F, I and J, and EV1A). In addition, Mts is required for initial dendrite arborization, as the number of primary and secondary dendrites was significantly reduced in *mts* RNAi or mutant neurons (Appendix Fig S1C). We also observed the simplified dendrite morphology in mts^{xe2258} mutant neurons from the wandering 3rd instar larvae, compared to that in the wild-type ones (Fig EV1B and C). Taken together, Mts is required for both dendrite pruning and initial dendrite arborization in ddaC neurons. To examine whether PP2A is required at the timing of pruning, and the dendrite pruning defect in *mts* mutant neurons is not caused by the initial morphology defect, we made use of the RU486-inducible GeneSwitch system [42] to induce a dominant-negative mutant form of Mts (Mts-dn) [36], which lacks the N-terminal region of its phosphatase domain. Mts-dn expression was induced from the 2nd instar stage upon RU486 feeding. While RU486 treatment did not alter the number of primary and secondary dendrites of Mts-dn-expressing ddaC neurons at the white prepupal (WP) stage (Fig 1G, H and K), severe dendrite pruning defects were observed at 16 h APF with 9.9 primary and secondary dendrites attached to the soma (Fig 1G, H and K).

Collectively, Mts acts as a new regulator that mediates dendrite pruning in a cell-autonomous manner during early metamorphosis.

The scaffolding subunit PP2A-29B is essential for ddaC dendrite pruning

The catalytic subunit of PP2A associates with the scaffolding subunit to form a core enzyme, which subsequently binds to the regulatory subunit to form the holoenzyme [43]. Given that PP2A-29B is the only known scaffolding subunit in *Drosophila*, we next examined a potential requirement of PP2A-29B for dendrite pruning. In contrast to the controls (Fig 2A), attenuation of *pp2a-29b* by three RNAi transgenes, v49671 (#1), v49672 (#2), and BSC29384 (#3), resulted in consistent dendrite pruning defects in ddaC neurons (Fig 2B, F and G, Appendix Fig S1B), similar to *mts* knockdown. Compared to the control clones (Fig 2C, F and G), ddaC MARCM clones derived from a lethal P-element insertion allele, $pp2a\text{-}29b^{rs}$, exhibited similar severing defects with full penetrance; 6.1 primary and secondary dendrites were attached to the soma at 16 h APF (Fig 2D, F and G). The expression of wild-type PP2A-29B protein in $pp2a\text{-}29b^{rs}$ mutant ddaC neurons completely rescued the dendrite pruning defects (Fig 2E–G). Thus, the scaffolding subunit PP2A-29B also plays an important role in dendrite pruning; the core PP2A enzyme consisting of Mts and PP2A-29B is critical for regulating dendrite pruning in ddaC sensory neurons.

Two regulatory subunits of PP2A, Wdb and Tws, are required for ddaC dendrite pruning

We next attempted to identify possible regulatory subunits of PP2A, which may act together with the core enzyme to regulate dendrite pruning. In *Drosophila*, there are four regulatory subunits for PP2A, including Tws, Wrd, Wdb, and PR72. We therefore knocked down

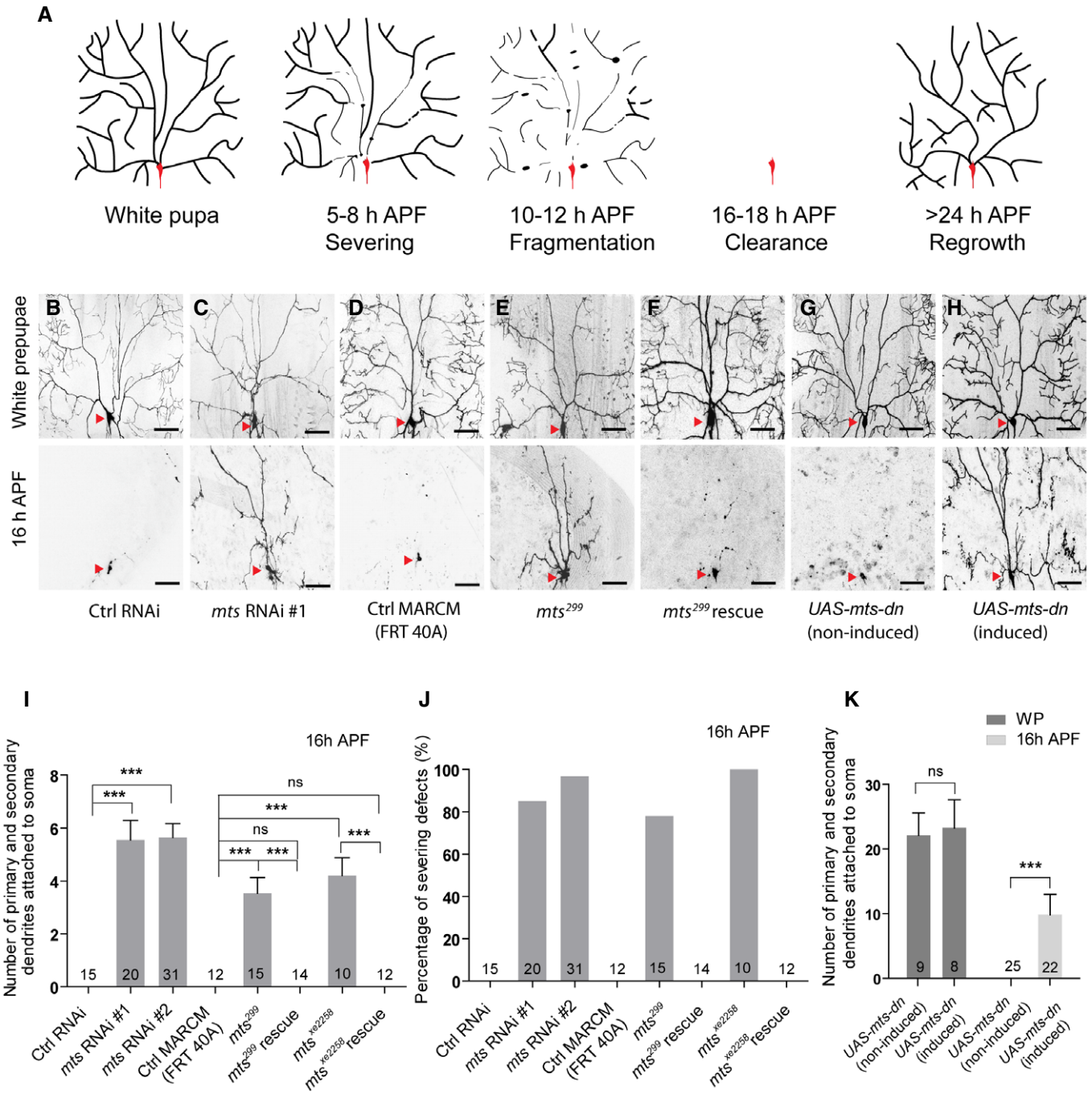

Figure 1. Mts is required for dendrite pruning in ddaC neurons.

A A Schematic representation of dendrite pruning in ddaC neurons.

B–F Live confocal images of ddaC neurons expressing UAS-mCD8-GFP driven by *ppk-Gal4* at WP and 16 h APF stages. Dendrites of ctrl RNAi (B), *mts* RNAi #1 (C), ctrl MARCM (D), mts^{299} MARCM (E), and mts^{299} rescue (F) ddaC neurons at WP and 16 h APF stages. Red arrowheads point to the ddaC somas.

G, H *UAS-mts-dn* ddaC neurons from animals in RU486-induced condition (H) driven by *GeneSwitch-Gal4-2295* exhibited normal arbors at WP stage and severe dendrite pruning defects at 16 h APF, compared to those in a non-induced condition (G). Red arrowheads point to the ddaC somas.

I–K Quantification of number of primary and secondary dendrites attached to soma and percentage of severing defects at 16 h APF.

Data information: In (I–K), data are presented as mean ± SEM from three independent experiments. One-way ANOVA with Bonferroni test (I) and two-tailed Student's *t*-test (K) were applied to determine statistical significance. ns, not significant; ***$P < 0.001$. The number of neurons (n) examined in each group is shown on the bars. Scale bars in (B–H) represent 50 μm.
Source data are available online for this figure.

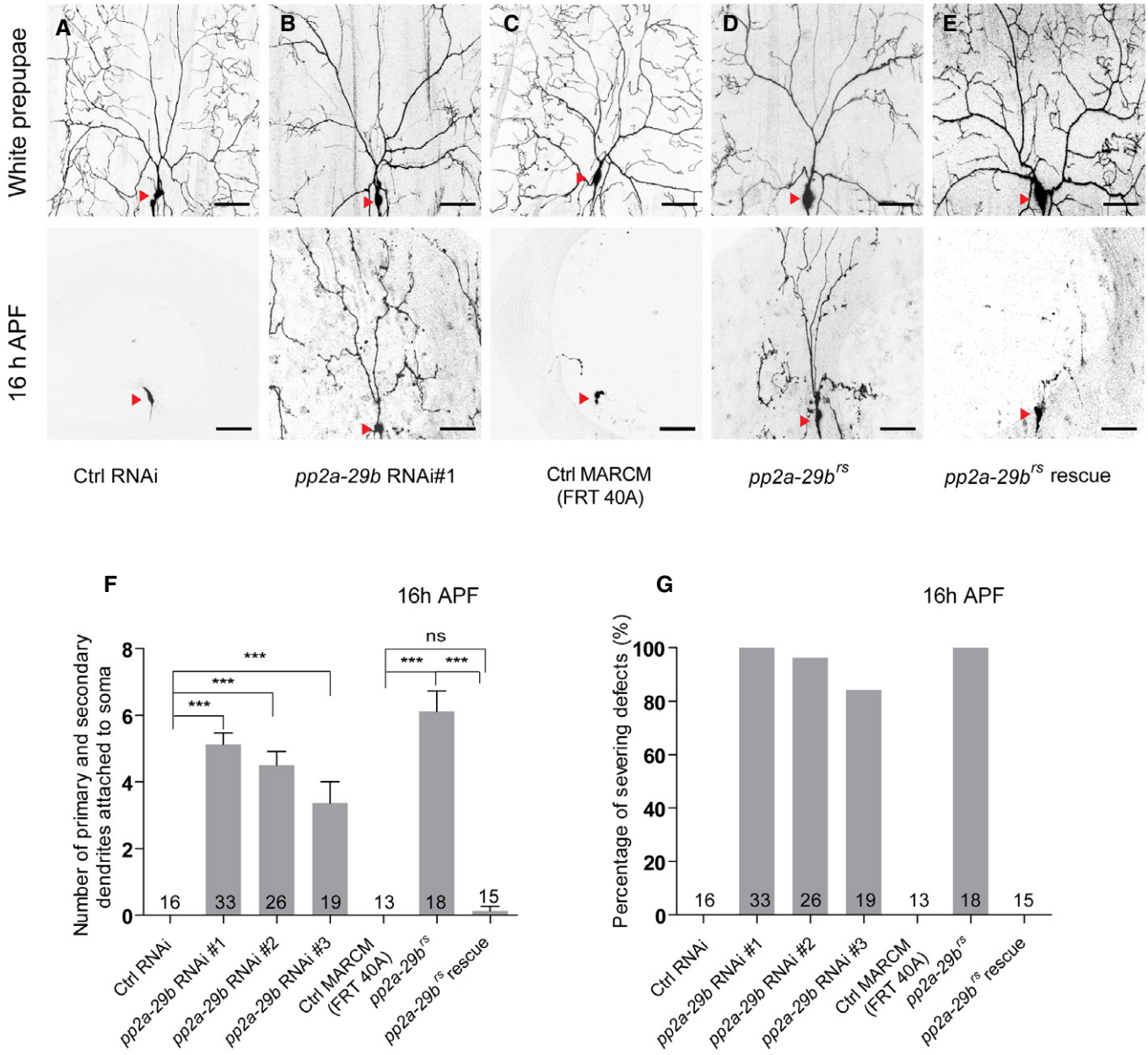

Figure 2. PP2A-29B is required for dendrite pruning in ddaC neurons.

A–E Live confocal images of ddaC neurons expressing UAS-mCD8-GFP driven by *ppk-Gal4* at WP and 16 h APF stages. Dendrites of ctrl RNAi (A), *pp2a-29b* RNAi #1 (B), ctrl MARCM (C), *pp2a-29b*^{rs} MARCM (D), and *pp2a-29b*^{rs} rescue (E) ddaC neurons at WP and 16 h APF stages. Red arrowheads point to the ddaC somas.

F, G Quantification of number of primary and secondary dendrites attached to soma and percentage of severing defects at 16 h APF.

Data information: In (F-G), data are presented as mean ± SEM from three independent experiments. ns, not significant; ***$P < 0.001$ (one-way ANOVA with Bonferroni test). The number of neurons (n) examined in each group is shown on the bars. Scale bars in (A–E) represent 50 μm.
Source data are available online for this figure.

all these regulatory subunits via a variety of available RNAi lines. Compared to the controls (Fig 3A), knockdown of either *wdb* or *tws* caused dendrite pruning defects (Figs 3B, C, I and J, and EV2A). Double knockdown of *wdb* (RNAi #1) and *tws* (RNAi #1) exacerbated the dendrite pruning phenotype, compared to either *wdb* or *tws* knockdown (Fig EV2B). To further confirm the requirement of *wdb* and *tws* in dendrite pruning, we conducted MARCM analyses using *wdb* or *tws* mutants. Compared to no pruning defect in the wild-type clones (Fig 3D, I and J), *wdb*^{dw} *and wdb*^{14} mutants exhibited the pruning defects in 91 and 100% of their ddaC mutant clones, which retained approximately 7.4 and 4.6 major dendrites, respectively (Fig 3E, F, I and J). Likewise, MARCM analysis of *tws*^{60}, a previously published allele [35], revealed consistent dendrite pruning defects in 41% of the mutant clones (Fig 3G, I and J), which

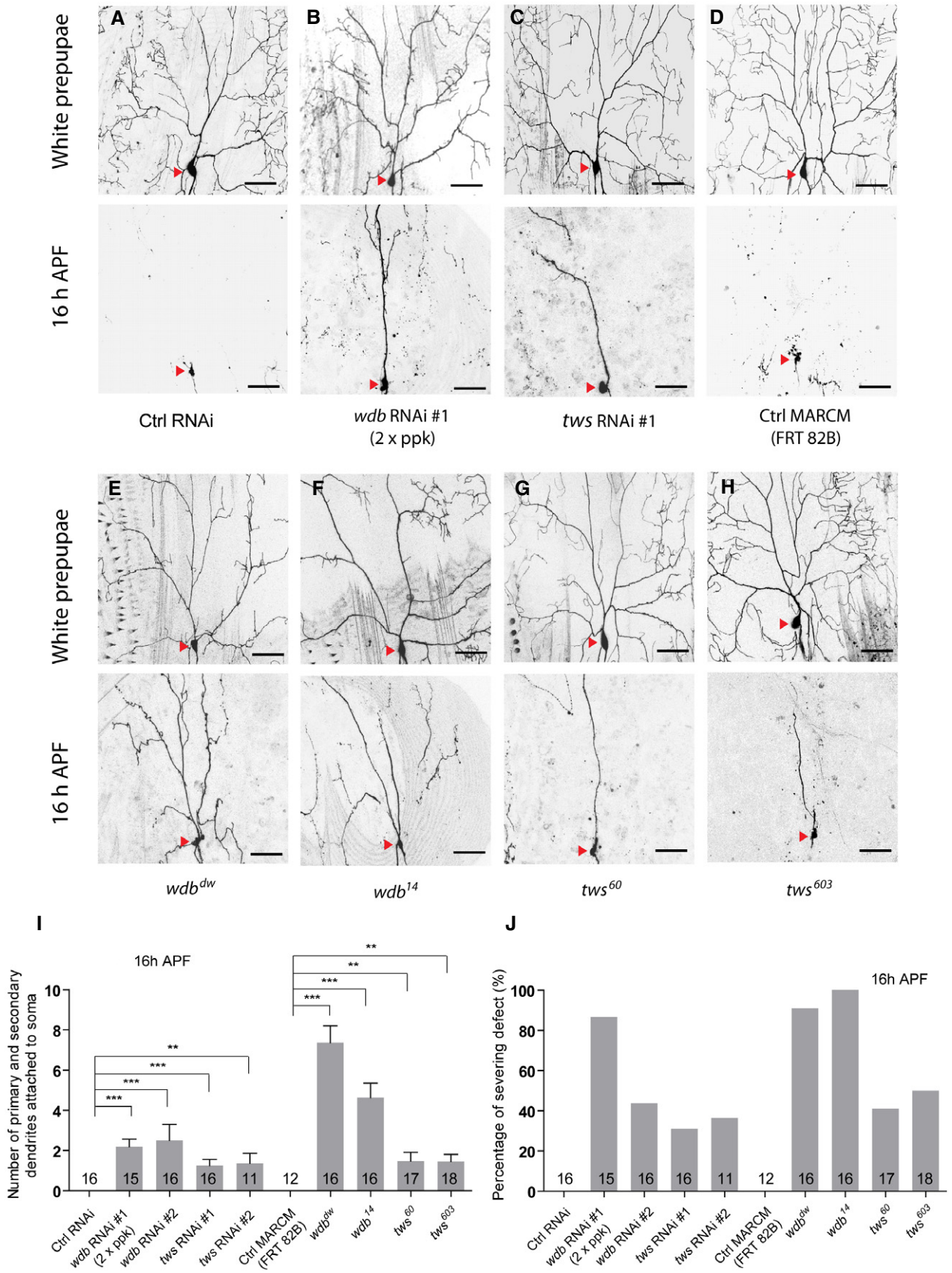
White prepupae
16 h APF
A
B
C
D
Ctrl RNAi
wdb RNAi #1
(2 x ppk)
tws RNAi #1
Ctrl MARCM
(FRT 82B)
E
F
G
H
wdb^dw
wdb^14
tws^60
tws^603
I
16h APF
Number of primary and secondary dendrites attached to soma
16 15 16 16 11 12 16 16 17 18
J
16h APF
Percentage of severing defect (%)
16 15 16 16 11 12 16 16 17 18

Figure 3.

Figure 3. Two regulatory subunits of the PP2A, Wdb and Tws, are required for ddaC dendrite pruning.

A–H Live confocal images of ddaC neurons expressing UAS-mCD8-GFP driven by *ppk-Gal4* at WP and 16 h APF stages. Dendrites of ctrl RNAi (A), *wdb* RNAi #1 driven by two copies of *ppk-Gal4* (B), *tws* RNAi #1 (C), ctrl MARCM (D), wdb^{dw} MARCM (E), wdb^{14} MARCM (F), tws^{60} MARCM (G), and tws^{603} MARCM (H) ddaC neurons at WP and 16 h APF stages. Red arrowheads point to the ddaC somas.

I, J Quantification of number of primary and secondary dendrites attached to soma and percentage of severing defects at 16 h APF.

Data information: In (I–J), data are presented as mean ± SEM from three independent experiments. $^{**}P < 0.01$; $^{***}P < 0.001$ (one-way ANOVA with Bonferroni test). The number of neurons (n) examined in each group is shown on the bars. Scale bars in (A–H) represent 50 μm.
Source data are available online for this figure.

appear to be weaker than those in *wdb* mutants. In a parallel clonal screen, we also isolated another new *tws* allele, tws^{603}, which showed similar dendrite pruning defects in 50% of its mutant clones (Fig 3H–J). Thus, these results show that two PP2A regulatory subunits, Wdb and Tws, are required to regulate ddaC dendrite pruning during metamorphosis.

We next investigated whether PP2A also regulates dendrite pruning of other da neurons during metamorphosis. Class I da neurons, ddaD and ddaE, undergo stereotyped dendrite pruning, similar to ddaC neurons. By 19 h APF, the dendrites of class I neurons were completely pruned in the wild-type animals (Appendix Fig S2A). In contrast, some dendritic branches of class I neurons remained attached to the soma in most of mts^{xe2258}, $pp2a\text{-}29b^{rs}$, or wdb^{dw} mutant neurons at the same time point (Appendix Fig S2B–D). Taken together, these findings indicate that PP2A is also required for dendrite pruning of class I da neurons.

PP2A is required for the expression of Sox14 and Mical, two downstream targets of ecdysone signaling during dendrite pruning

Our previous studies have demonstrated that dendrite pruning of ddaC neurons requires the activation of ecdysone signaling which leads to upregulation of two downstream targets, the key transcription factor Sox14 and the actin regulators Mical [14]. We next investigated whether PP2A modulates the ecdysone pathway during dendrite pruning. To this end, we first examined the protein levels of EcR-B1, a neuron-specific ecdysone receptor, in various *PP2A* mutant ddaC neurons. Compared to the wild-type controls (Fig 4A and P), the levels of EcR-B1 protein were reduced in MARCM ddaC clones from mts^{xe2258} (Fig 4D and P) or $pp2a\text{-}29b^{rs}$ mutant (Fig 4G and P) and Mts-dn-overexpressing ddaC neurons (Appendix Fig S3A) at WP stage. It has been documented that Sox14 and Mical are dramatically upregulated in protein level during the larval–pupal transition [14]. Interestingly, compared to that in the control neurons (Fig 4B and Q), Sox14 protein levels were reduced at WP stage in the ddaC clones derived from mts^{xe2258} (Fig 4E and Q), $pp2a\text{-}29b^{rs}$ (Fig 4H and Q), or *mts-dn* neurons (Appendix Fig S3A), suggesting that Mts and PP2A-29B are required for the upregulation of Sox14 protein expression prior to dendrite pruning. Given that Sox14 is critical for upregulation of the actin regulator Mical, we next investigated Mical levels in *mts* or *pp2a-29b* mutant neurons at WP stage. In the wild-type neurons, Mical protein was abundantly expressed at WP stage (Fig 4C and R). Similar to Sox14, Mical protein levels were reduced in ddaC neurons from mts^{xe2258} (Fig 4F and R), $pp2a\text{-}29b^{rs}$ (Fig 4I and R), *or mts-dn* (Appendix Fig S3A) mutant neurons at WP stage. Using a *mical-β-gal* reporter that drives the LacZ expression in ddaC neurons under the control of a *mical* enhancer [16], the LacZ expressions were absent or strongly reduced in *mts* or *pp2a-29b* RNAi neurons (Appendix Fig S3B). These data suggest that Mts and PP2A-29B likely regulate the transcription of *mical* in ddaC neurons. Interestingly, EcR-B1 protein levels appeared to be unchanged in wdb^{dw} (Fig 4J and P) or wdb^{14} neurons (Appendix Fig S3A). In contrast, either Sox14 or Mical expression levels were significantly reduced in wdb^{dw} (Fig 4K, L Q and R) or wdb^{14} neurons (Appendix Fig S3A). Moreover, tws^{60} MARCM ddaC clones did not exhibit a significant alteration in the levels of EcR-B1 (Fig 4M and P), Sox14 (Fig 4N and Q), and Mical (Fig 4O and R) at WP stage. Taken together, these results suggest that PP2A, via Wdb, regulates the expression of Sox14 and Mical to facilitate ecdysone signaling in ddaC neurons prior to dendrite pruning.

We further tested whether PP2A regulates dendrite pruning through upregulation of Mical protein. We overexpressed Mical protein via a *UAS-mical* transgene in mts^{299}, $pp2a\text{-}29b^{rs}$, or *wdb* RNAi ddaC neurons to assess if overexpressed Mical is able to suppress their dendrite pruning defects. The wild-type clones or control RNAi neurons completely removed their larval dendrites (Fig 5A, D and G). Interestingly, the pruning defects associated with mts^{299} (Fig 5B, J and K), $pp2a\text{-}29b^{rs}$ (Fig 5E, J and K), or *wdb* RNAi (Fig 5H, J and K) mutant neurons were significantly suppressed by the overexpression of Mical at 16 h APF (Fig 5C, F and I–K). Thus, these data suggest that PP2A controls dendrite pruning of ddaC neurons at least partially via Mical upregulation.

Figure 4. PP2A is required to regulate ecdysone signaling during dendrite pruning.

A–O Confocal images of control (A–C), mts^{xe2258} (D–F), $pp2a\text{-}29b^{rs}$ (G–I), wdb^{dw} (J–L), and tws^{60} (M–O), MARCM ddaC clones that were immunostained for EcR-B1 (A, D, G, J, M) and Sox14 (B, E, H, K, N), and Mical (C, F, I, L, O) at WP stage. ddaC somas are labeled by dashed lines, ddaE by asterisks. ddaC neurons were identified by *ppk-Gal4*-driven mCD8::GFP (green channel) expression, as shown at the top right corner.

P–R Quantitative analyses of normalized EcR-B1, Sox14, and Mical fluorescence intensities in ddaC neurons.

Data information: In (P–R), data are presented as mean ± SEM from three independent experiments. ns, not significant; $^{*}P < 0.05$; $^{***}P < 0.001$ (one-way ANOVA with Bonferroni test). The number of neurons (n) examined in each group is shown on the bars. Scale bars in (A–O) represent 10 μm.
Source data are available online for this figure.

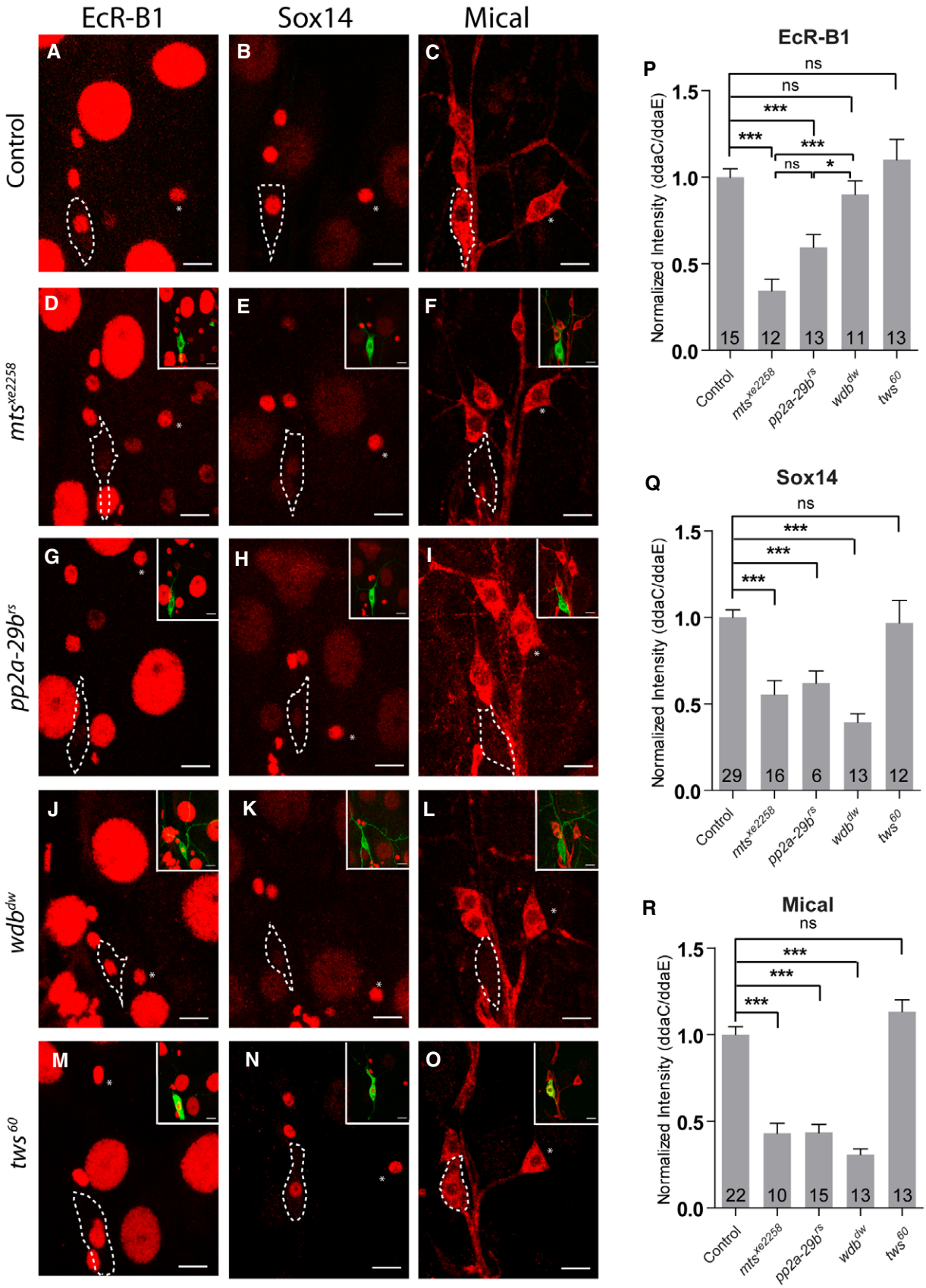

Figure 4.

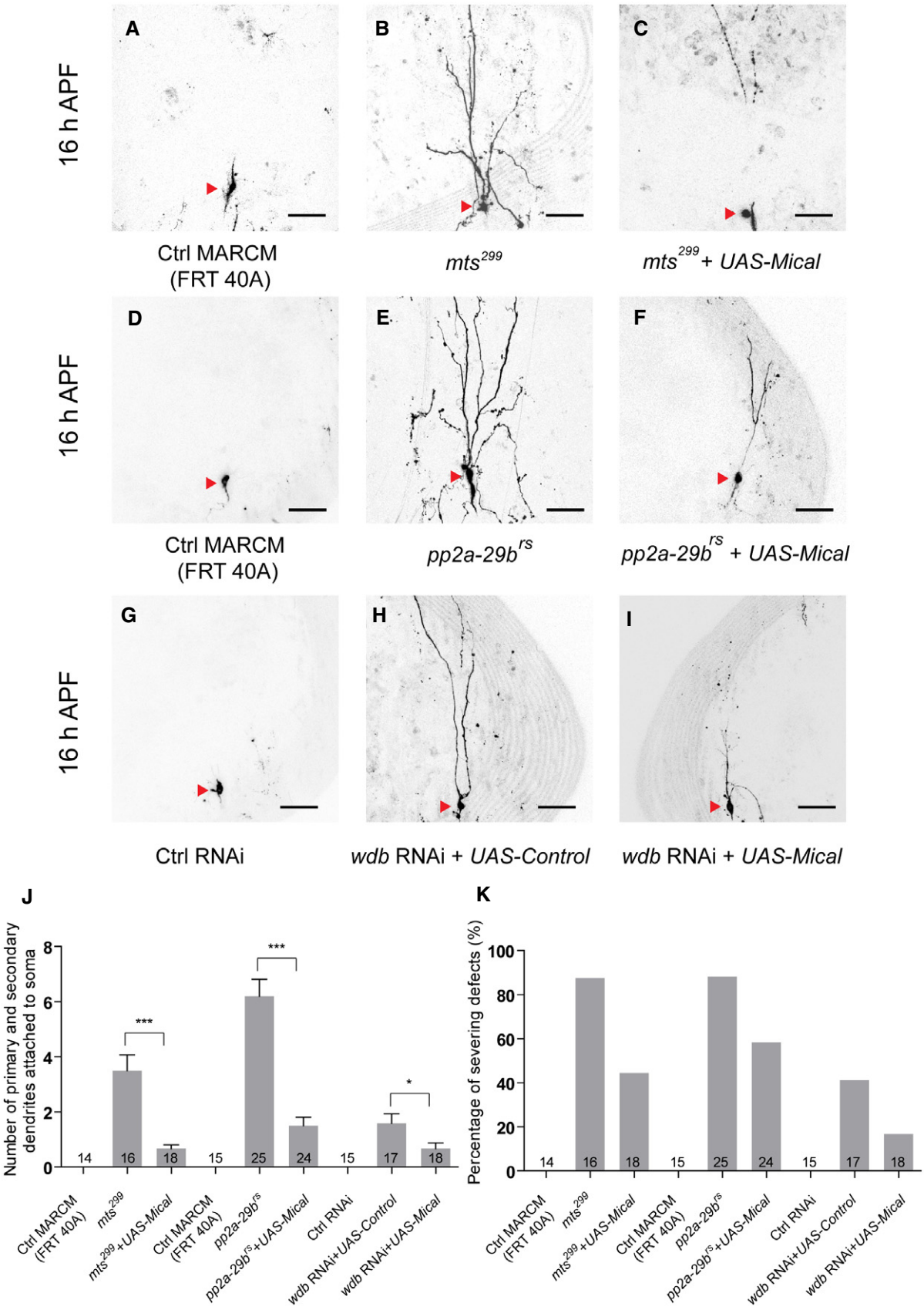

Figure 5.

Figure 5. Mical overexpression significantly suppressed the dendrite pruning defects in *PP2A* mutant neurons.

A–I Live confocal images of ddaC neurons expressing UAS-mCD8-GFP driven by *ppk-Gal4* at WP and 16 h APF stages. Dendrites of ctrl MARCM (A), mts^{299} MARCM (B), *UAS-Mical* + mts^{299} MARCM (C), ctrl MARCM (D), $pp2a\text{-}29b^{rs}$ MARCM (E), *UAS-Mical* + $pp2a\text{-}29b^{rs}$ MARCM (F), ctrl RNAi (G), *wdb* RNAi + *UAS-Control* (H), and *wdb* RNAi + *UAS-Mical* (I) ddaC neurons at 16 h APF stage. Red arrowheads point to the ddaC somas.

J, K Quantification of number of primary and secondary dendrites attached to soma and percentage of severing defects at 16 h APF.

Data information: In (J–K), data are presented as mean ± SEM from three independent experiments. *$P < 0.05$; ***$P < 0.001$ (two-tailed Student's *t*-test). The number of neurons (n) examined in each group is shown on the bars. Scale bars in (A–I) represent 50 μm.
Source data are available online for this figure.

PP2A is required for proper distribution of dendritic and axonal MT markers

It has been shown that Mical functions as an actin disassembly factor to disassemble F-actin *in vitro* and in bristles [44]. However, we did not observe any obvious defect in the phalloidin staining in the proximal dendrites and soma of *mts* and *pp2a-29b* RNAi ddaC neurons from the 3rd instar larvae (Fig EV3A and B), suggesting that PP2A does not regulate overall F-actin level. However, PP2A is shown to modulate F-actin dynamics in a separate study [45]. Recent studies have also documented that MT dynamics, stability, and orientation play important roles in dendrite pruning [17,21–23]. Since PP2A can regulate the structure of MT cytoskeleton in motor neurons [39], we then proceeded to investigate its potential role in regulating MTs in ddaC sensory neurons. We examined the distribution/level of MT-associated proteins (Patronin, TACC and Mini spindles/Msps) as well as two MT markers (Nod-β-gal and Kin-β-gal; also known as Khc::Nod::LacZ and Khc::LacZ, respectively) when PP2A subunits were depleted. While the levels/distributions of Patronin, TACC, and Msps appeared to be normal (Appendix Fig S4A and B), the distributions of Nod-β-gal and Kin-β-gal were drastically affected in various *PP2A* mutant or RNAi neurons (Fig 6). The chimera Nod-β-gal, which consists of the Nod motor domain (residues 1–320), the kinesin-1 coiled-coil domain (residues 334–606), and the β-galactosidase (β-gal) tag, was previously used as a marker to label the sites enriched with the MT minus ends in multiple *Drosophila* cell types [46,47]. In sensory neurons, Nod-β-gal was specifically enriched in dendrites but absent in axons and thus used as a marker for potentially detecting the presence of minus-end-out MTs in dendrites [23,47–49]. Nod-β-gal was localized in the dendrites, but not in the axons, of the control ddaC neurons (Fig 6A, Appendix Fig S5A and B). Strikingly, Nod-β-gal signals were significantly reduced in the dendrites but highly enriched in the soma when Mts (Fig 6B, K and L), PP2A-29B (Fig 6C, K and L), or Tws (Fig 6D, K and L) were knocked down in ddaC neurons. Consistent with the RNAi knockdown, ddaC clones from tws^{603} mutant also exhibited a strong reduction in the dendrites but an accumulation in the soma in terms of Nod-β-gal levels (Appendix Fig S5A and Fig 6K and L). To quantify the alterations of dendritic Nod-β-gal distribution, we measured the intensity of β-gal fluorescence in the dendrites that are 30 μm away from the soma. In *mts* RNAi, *pp2a-29b* RNAi, and tws^{603} mutant neurons, dendritic Nod-β-gal signals were significantly reduced to approximately 10–20% of the original level (Fig 6K), suggesting drastic decreases in dendritic minus-end-out MTs. Interestingly, the Nod-β-gal distribution was not affected in wdb^{dw} mutant clones (Fig 6E, K and L). Overexpression of Mical did not rescue the defective Nod-β-gal distribution in *tws* RNAi neurons (Appendix Fig S5B). Thus, these data indicate that PP2A might regulate dendritic MT orientation through the regulatory subunit Tws but not Wdb.

We next detected the localization of the axon-specific marker Kin-β-gal, in which the motor and coiled-coil domains of kinesin-1 (residues 1–606) are fused with the β-gal tag. Kin-β-gal localizes at the sites enriched with MT plus ends [46]. In the wild-type ddaC neurons, the Kin-β-gal signals were detectable in the axons but not in the dendrites (Fig 6F) [23,47], suggesting the presence of plus-end-out MTs predominantly in axons. Notably, punctate Kin-β-gal signals were observed in the dendrites of *mts* (Fig 6G and M), *pp2a-29b* (Fig 6H and M), or *tws* (Fig 6I and M) RNAi ddaC neurons, suggesting the presence of plus-end-out MTs in the mutant dendrites. However, Kin-β-gal was properly localized in the axons of wdb^{dw}/wdb^{14} mutant neurons (Fig 6J and M). Thus, Wdb is dispensable for the distribution of Nod-β-gal and Kin-β-gal in dendrites and axons, respectively.

Taken together, Mts, PP2A-29B, and Tws govern proper distribution of dendrite and axon-specific MT markers in ddaC neurons.

Figure 6. PP2A is essential for proper distribution of dendritic and axonal MT markers.

A–E Confocal images of ddaC neurons at the wandering 3rd instar (wL3) stage immunostained for anti-β-galactosidase. Nod-β-gal signals were localized in the dendrites of the ctrl RNAi (A) and wdb^{dw} (E) mutant ddaC neurons; however, Nod-β-gal levels were strongly reduced in the dendrites and accumulated in the somas in *mts* RNAi (B), *pp2a-29b RNAi* (C), and *tws RNAi* (D) ddaC neurons. ddaC somas are marked by asterisks, axons by arrows, and dendrites used for analyzing by curly brackets.

F–J Kin-β-gal was mislocalized to the dendrites in *mts* RNAi (G), *pp2a-29b RNAi* (H), *tws* RNAi (I), and wdb^{dw}/wdb^{14} (J) mutant ddaC neurons, compared to the ctrl RNAi neurons (F), while the localization of Kin-β-gal in wdb^{dw}/wdb^{14} mutant (J) is normal. ddaC somas are marked by asterisks, axons by arrows, and white arrowheads point to dendritic Kin-β-gal signals.

K Quantification of normalized Nod-β-gal fluorescence intensity in dendrites ofddaC neurons.

L, M Quantification of the percentage of neurons with defective Nod-β-gal and Kin-β-gal distribution in ddaC neurons.

Data information: In (K–M), data are presented as mean ± SEM from three independent experiments. ns, not significant; ***$P < 0.001$ (one-way ANOVA with Bonferroni test). The number of neurons (n) examined in each group is shown on the bars. Scale bars in (A–J) represent 10 μm.
Source data are available online for this figure.

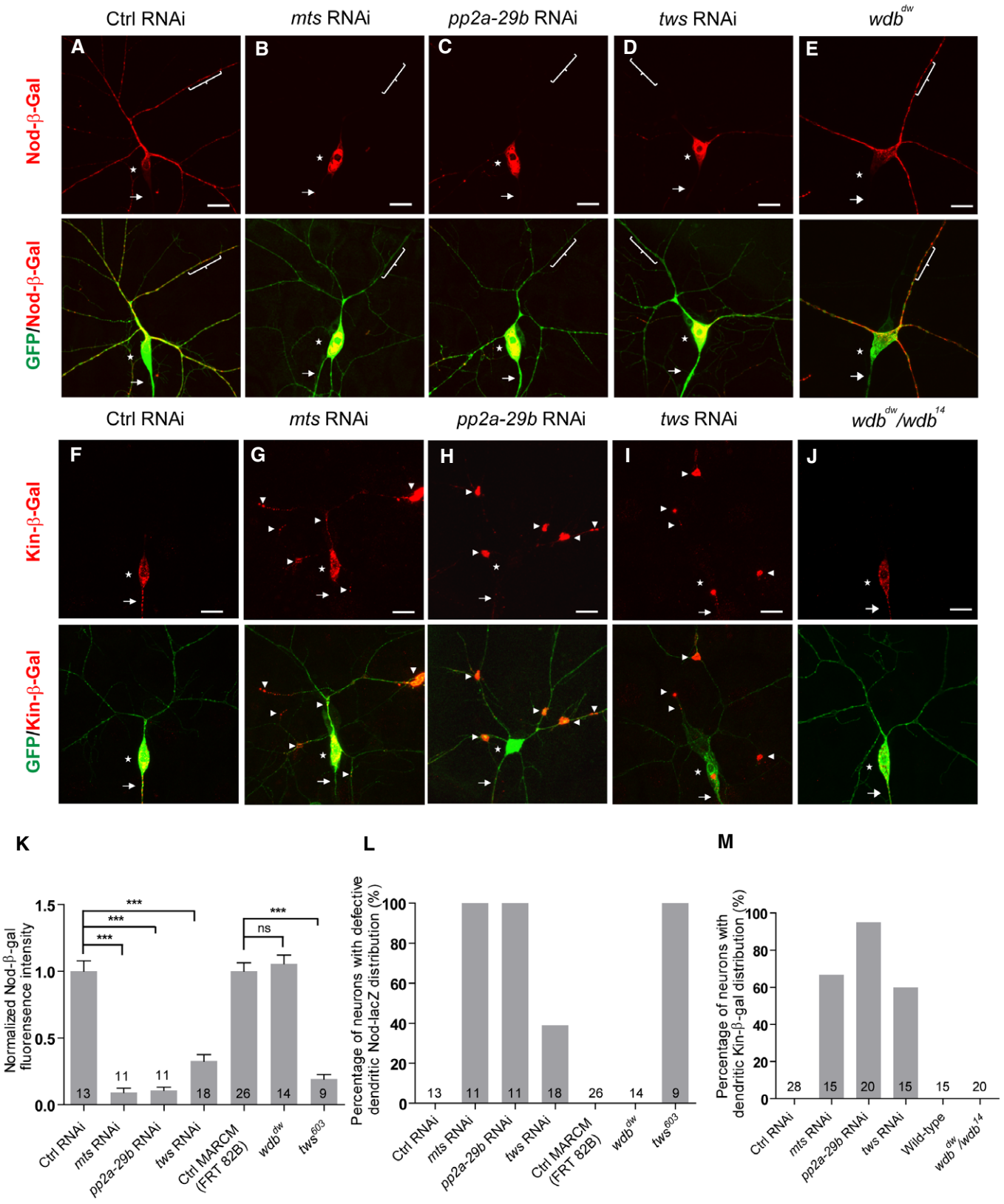

Figure 6.

PP2A is required for uniform minus-end-out MT orientation in the dendrites

Given that Nod-β-gal and Kin-β-gal distributions were impaired in the dendrites of *PP2A* mutant neurons, we next made use of the MT plus-end marker EB1-GFP to precisely determine dendritic MT orientation via live imaging. EB1-GFP marks growing plus ends of MTs; the direction of EB1-GFP movement is defined as MT orientation in neurons [49–51]. In *Drosophila* da neurons, > 95% of dendritic EB1-GFP comets move toward the soma (retrograde), whereas almost all axonal EB1-GFP comets migrate away from the soma (anterograde), suggesting a nearly uniform minus-end-out MT orientation in dendrites and a plus-end-out MT orientation in axons [52,53]. To determine whether PP2A regulates dendritic MT orientation, we set out to observe sequential MT growth by detecting the moving EB1-GFP comets in the dendrites of ddaC neurons. In the control ddaC neurons, almost all of dendritic EB1-GFP comets migrated toward the soma (retrograde), whereas approximately 1% of the dendritic comets moved away from the soma (anterograde) (Fig 7A and E, Appendix Fig S6A and B), indicating a uniform minus-end-out MT orientation in the major dendrites. In contrast, RNAi knockdown of *mts* or *pp2a-29b* led to approximately 16-fold and 20-fold increases, respectively, in the percentage of anterogradely moving comets (Fig 7B, C and E). Likewise, we also observed a similar defect in dendritic MT orientation in Mts-dn-overexpressing ddaC neurons (Appendix Fig S6A). Moreover, knockdown of Tws led to mixed MT orientations in the dendrites of ddaC neurons (Fig 7D and E). We observed an 8.5-fold increase in the percentage of anterograde EB1-GFP comets in the dendrites of *tws* RNAi neurons (Fig 7E). Similar to that in the wild-type neurons (Fig 7I and K), the minus-end-out MT orientation was not disturbed in the dendrites of wdb^{dw}/wdb^{14} mutant neurons (Fig 7J and K), confirming that Wdb is not important for dendritic MT orientation in ddaC neurons. In addition, knockdown of *wdb* in the *tws* RNAi background did not significantly enhance the dendritic MT misorientation phenotype (Appendix Fig S6B), suggesting that Tws and Wdb unlikely act redundantly to regulate dendritic MT orientation. We also measured the number, track length, and speed of EB1-GFP comets, which reflect overall MT dynamics and nucleation. In *mts*, *pp2a-29b*, *tws* RNAi, or *wdb* mutant neurons, we observed no or neglectable alterations on the number, track length, and speed of the EB1-GFP comets (Fig 7F–H and L–N).

Collectively, these data suggest that PP2A, via the regulatory subunit Tws but not Wdb, regulates the minus-end-out MT orientation in ddaC dendrites.

PP2A regulates dendritic MT orientation through suppressing Klp10A level

To gain insight into the molecular mechanism of PP2A in the regulation of dendritic MT orientation, we analyzed the level and localization of several MT regulators including Patronin, Klp10A, TACC, and Msps. Klp10A levels were significantly elevated upon *mts* or *pp2a-29b* knockdown (Fig 8A and B), whereas the rest of MT regulators remained unchanged (Appendix Fig S4A and B). We observed a 2.3-fold increase in Klp10A levels in the soma of *mts* RNAi ddaC neurons (Fig 8A and B), when compared to the controls. Klp10A levels were also significantly increased in the soma of *pp2a-29b* RNAi ddaC neurons (Fig 8A and B). Klp10A is a kinesin-13-family MT depolymerase that has been reported to regulate MT orientation in the dendrites of ddaC neurons [23]. Thus, PP2A appears to negatively regulate Klp10A level. To confirm the specificity of Klp10A signals, we further knocked down Klp10A in *mts* RNAi ddaC neurons. Knockdown of Klp10A strongly eliminated its signals in *mts* RNAi neurons (Fig EV4A and B), confirming that the Klp10A levels are elevated upon Mts knockdown. Likewise, knockdown of either Mts or PP2A-29B in class I ddaD/E neurons also exhibited a significant increase in Klp10A levels (Fig EV4C and D), suggesting a general role of PP2A in suppressing Klp10A level in sensory neurons. Klp10A level was not affected in wdb^{dw} ddaC clones (Fig EV4E and F). Similar to Wdb, Mical is not required to regulate Klp10A level and dendritic MT orientation, as knockdown of Mical did not affect the Klp10A level (Fig EV4G and H), Nod-β-gal distribution (Appendix Fig S7A), or EB1-GFP comet directionality (Appendix Fig S7B).

To examine whether the MT orientation defects in *mts* RNAi or *pp2a-29b* RNAi neurons are caused by elevated Klp10A level, we further attenuated Klp10A in these RNAi neurons and examined dendritic MT orientation. Klp10A knockdown almost completely restored the retrograde movement of dendritic EB1-GFP comets in *mts* RNAi ddaC neurons (Fig 8C and D). Likewise, Klp10A knockdown led to a significant reduction in the percentage of anterograde EB1-GFP comets in the *pp2a-29b* RNAi ddaC dendrites (Fig 8E and F). Consistently, knocking down *klp10A* in *tws* RNAi ddaC neurons

Figure 7. PP2A is required for uniform minus-end-out orientation of dendritic MTs in ddaC neurons.

A–D Representative kymographs depicting the movement patterns of EB1 comets in the proximal dendrites of ddaC neurons at 96 h AEL. In control RNAi (A) ddaC dendrites, EB1-GFP comets predominantly moved toward the somas (retrograde). However, in *mts* RNAi (B), *pp2a-29b* RNAi (C), and *tws* RNAi (D) ddaC dendrite branches, some EB1-GFP comets moved away from the somas (anterograde).

E–H Quantitative analyses of the percentages of anterograde EB1 comets in each neuron imaged (E), the average numbers of EB1-GFP comets within 30 μm dendrite in 3 min (F), the average comet track length of each neuron (G), and the average comet speed of each neuron (H).

I, J Representative kymographs depicting the movement patterns of EB1 comets in the proximal dendrites of ddaC neurons at 96 h AEL. In both control (I) and wdb^{dw}/wdb^{14} mutant (J) ddaC dendrites, EB1-GFP comets predominantly moved toward the somas (retrograde).

K–N Quantitative analyses of the percentages of anterograde EB1 comets in each neuron imaged (K), the average numbers of EB1-GFP comets within 30 μm dendrite in 3 min (L), the average comet track length of each neuron (M), and the average comet speed of each neuron (N).

Data information: In (E–H) and (K–N), data are presented as mean ± SEM from three independent experiments. ns, not significant; $*P < 0.05$; $***P < 0.001$ (E–H, one-way ANOVA with Bonferroni test; K–N, two-tailed Student's *t*-test). The number of neurons (n) examined in each group is shown on the bars. Horizontal arrow indicates the direction toward the somas, and vertical arrow indicates that each movie was taken for 3 min. Scale bars in (A, I) represent 10 μm.
Source data are available online for this figure.

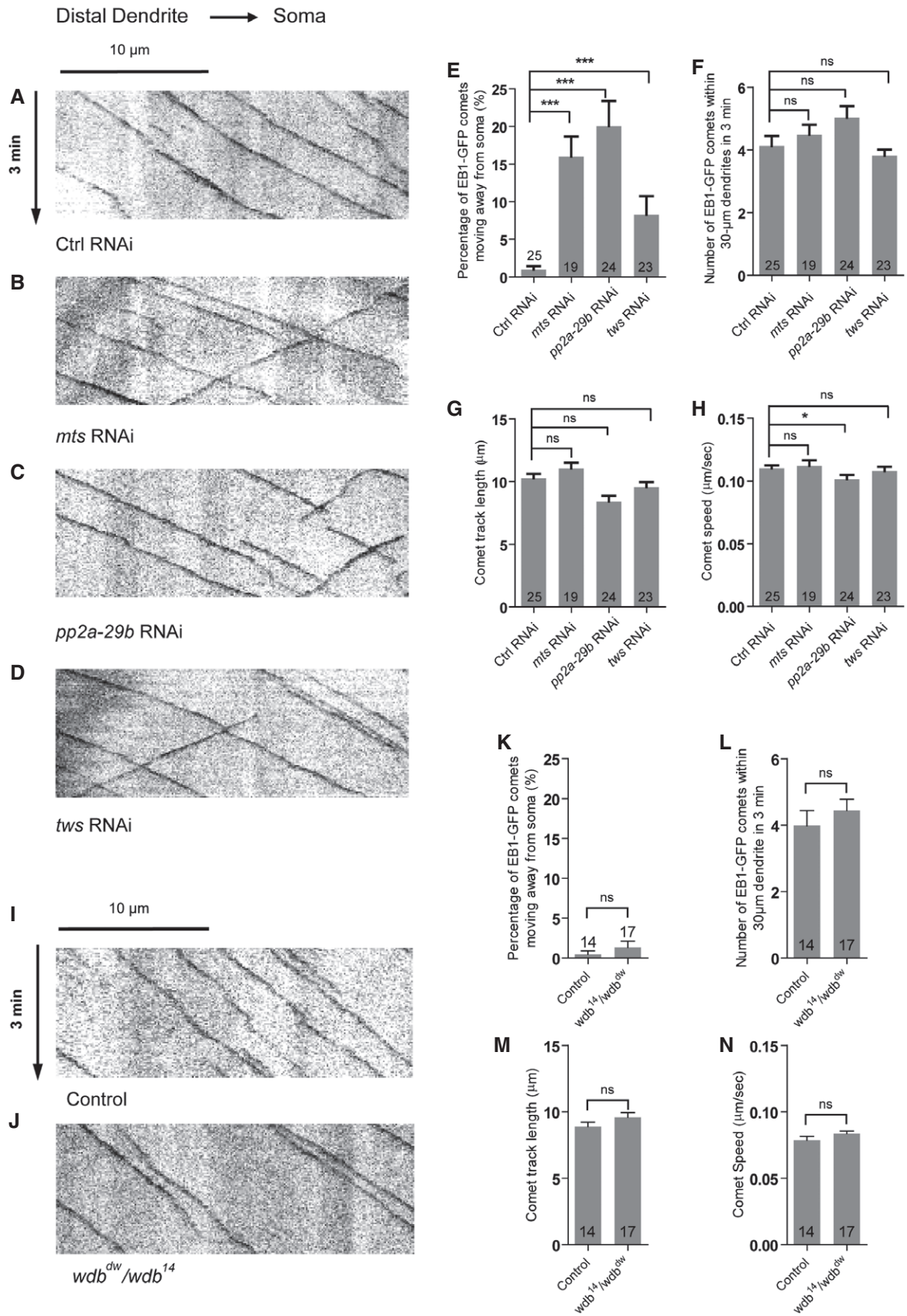

Figure 7.

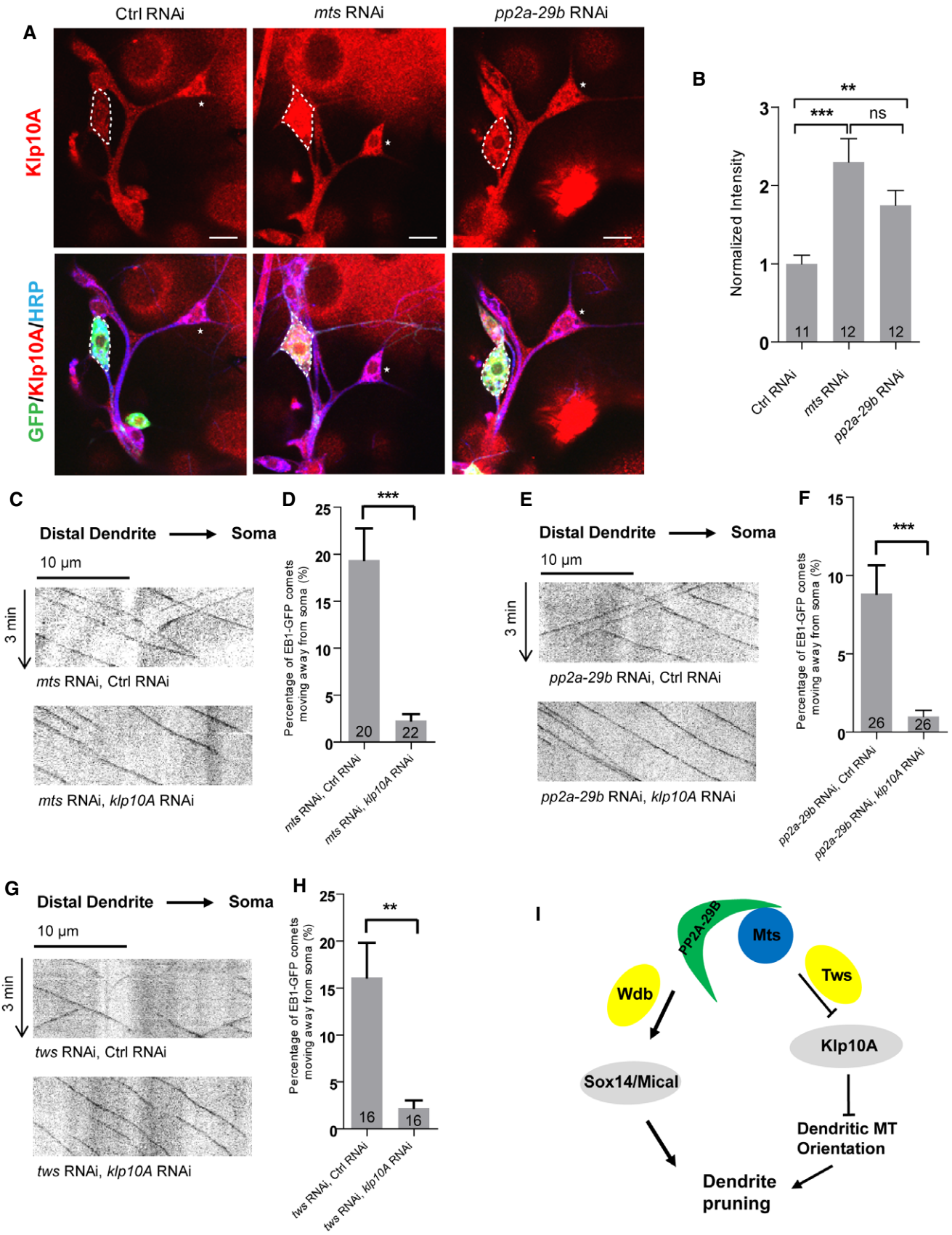

Figure 8.

Figure 8. PP2A regulates dendritic MT orientation through suppressing Klp10A levels.

A Confocal images of ctrl RNAi, *mts* RNAi, and *pp2a-29b* RNAi ddaC neurons immunostained for Klp10A at wL3 stages. ddaC somas are labeled by dashed lines; ddaE somas are marked by asterisks.

B Quantitative analysis of normalized Klp10A fluorescence intensities of ddaC somas.

C–H Representative kymographs depicting the movement patterns of EB1 comets in the proximal dendrites of ddaC neurons at 96 h AEL in (C) *mts* RNAi + ctrl RNAi and *mts* RNAi + *klp10a* RNAi; (E) *pp2a-29b* RNAi + ctrl RNAi and *pp2a-29b* RNAi + *klp10a* RNAi; and (G) *tws* RNAi + control RNAi and *tws* RNAi + *klp10a* RNAi. (D, F, H) Quantitative analyses of the percentages of anterograde EB1 comets in ddaC neurons.

I A possible model. PP2A, via Wdb, regulates ddaC dendritepruning through the expression of Sox14 and Mical, whereas PP2A, via Tws, regulates dendritic MT polarity via suppressing the Klp10A levels.

Data information: In (B, D, F, H), data are presented as mean ± SEM from three independent experiments. ns, not significant; $^{**}P < 0.01$; $^{***}P < 0.001$ (B, one-way ANOVA with Bonferroni test; D, F, H, two-tailed Student's *t*-test). The number of neurons (n) examined in each group is shown on the bars. Scale bars in (A, C, E, G) represent 10 μm. (C, E, G) Horizontal arrow indicates the direction toward the somas, and vertical arrow indicates that each movie was taken for 3 min.
Source data are available online for this figure.

almost fully rescued the dendritic MT orientation defects (Fig 8G and H). Thus, mixed MT orientations in the dendrites of *PP2A* RNAi neurons are likely caused by elevated Klp10A level or activity. Moreover, Klp10A knockdown slightly suppressed the dendrite pruning defects in *mts* or *pp2a-29b* RNAi neurons (Fig EV5A), however, did not restore Mical expression (Fig EV5B). The partial suppression suggests that PP2A regulates dendrite pruning partly via Klp10-mediated MT orientation.

Discussion

Pruning is essential for the development and refinement of neuronal circuits [54]. During *Drosophila* metamorphosis, ddaC neurons selectively eliminate their dendrites while keeping their axons intact. Recent studies report that PP2A dysfunction is associated with a series of neurodegenerative diseases in humans, such as Parkinson's disease and Alzheimer's disease [55,56]. In this study, we identified *Drosophila* PP2A as an important regulator of dendrite pruning during development. We first isolated the catalytic subunit Mts, the scaffolding subunit PP2A-29B, and two regulatory subunits, namely Wdb and Tws. Our data suggest that PP2A, via Wdb, facilitates the expression of Sox14 and Mical, two downstream targets of ecdysone signaling, whereas PP2A, via Tws, regulates dendritic minus-end-out MT orientation which is required for dendrite pruning [23] (see the model in Fig 8I).

PP2A regulates ecdysone signaling during dendrite pruning

In this study, we found that the dendrite pruning phenotypes in various *pp2a* mutants are reminiscent of those of *EcR*, *sox14,* or *mical* mutants [9,10,14]. Indeed, both Mts and PP2A-29B are required to upregulate the expression of EcR-B1, Sox14, and Mical in ddaC neurons. Furthermore, PP2A promotes dendrite pruning via the activation of Mical expression, as Mical overexpression dramatically suppressed the dendrite pruning defects in *mts* and *pp2a-29b* mutant neurons. Different from the catalytic (Mts) and scaffolding subunits (PP2A-29B), the regulatory subunit Wdb is important for Sox14 and Mical expression, but appears dispensable for EcR-B1 expression. Wdb might regulate Sox14 and Mical expression in parallel to or downstream of EcR-B1. Alternatively, multiple regulatory subunits of PP2A might act redundantly with Wdb to facilitate EcR-B1 expression. How PP2A regulates EcR-B1 expression remains unclear. EcR-B1 expression is induced by the TGF-β signaling, the cohesion complex, and the nuclear receptors Ftz-f1/Hr39 before the onset of axon pruning in mushroom body γ neurons [57–59], which are likely conserved in ddaC neurons. We speculate that PP2A may regulate the expression of EcR-B1 via the modulation of its upstream regulators/pathways, for example, TGF-β pathway and the cohesin complex. It has been reported that phosphorylation of TGF-β receptors and cohesin is important for their functions [60,61]. PP2A might modulate their phosphorylation levels to elicit their downstream pathways including ecdysone signaling.

PP2A regulates dendritic MT polarity by inhibiting the MT-depolymerizing kinesin Klp10A

During dendrite pruning, MT breakdown appears to precede the scission of dendritic membrane in ddaC neurons, leading to severing of proximal dendrites from the soma [10,17]. Growing evidence indicates that regulators of MT cytoskeletons are involved in dendrite pruning. Par-1 kinase promotes MT breakdown probably via Tau phosphorylation and thereby facilitates dendrite pruning of ddaC neurons [22]. Moreover, recent studies from us and others have demonstrated a high correlation between dendritic minus-end-out orientation and dendrite pruning. Kinesin-1/2 motors and a MT minus-end-binding protein Patronin regulate minus-end-out MT orientation in dendrites and are required for dendrite pruning in ddaC neurons [21,23,29,62]. The kinesin-13 MT depolymerase Klp10A antagonizes the function of Patronin and thereby negatively regulates dendritic MT orientation during dendrite pruning [23]. In addition, other regulators of dendritic MT polarity, for example, CNN and APC1/2 [52,63], appear to be required for dendrite pruning in ddaC neuron [23].

In this study, we report that PP2A also regulates both dendritic MT orientation and dendrite pruning in ddaC neurons. We observed Nod-β-gal/Kin-β-gal mislocalization as well as mixed EB1-GFP comets in the dendrites of *mts*, *pp2a-29b,* and *tws* RNAi neurons, suggesting increased plus-end-out MTs in mutant dendrites. These results raise the possibility that PP2A may regulate polarized MT nucleation and/or proper distribution of the MT nucleator γ-tubulin in the dendrites of ddaC neurons. Golgi outposts have been reported to locally nucleate MTs in the dendrites of sensory neurons [64], but a recent study suggested otherwise [53]. γ-tubulin might be associated with intracellular membrane of different organelles, for example, Golgi and the endoplasmic reticulum, to nucleate minus-end-out MTs in dendrites. PP2A might be involved in the proper distribution of γ-tubulin in dendrites and thereby cause polarized MT polymerization. Moreover, we found that PP2A regulates dendritic MT orientation and dendrite pruning at least partially via

suppressing the levels or functions of Klp10A. Klp10A protein levels were significantly elevated in *mts* or *pp2a-29b* RNAi neurons. Further knockdown of *klp10a* suppressed the defects in both dendritic MT orientation and dendrite pruning in these RNAi backgrounds. Therefore, loss of PP2A function phenocopies Klp10A overexpression in terms of dendrite pruning and dendritic MT orientation [23]. It is conceivable that elevated Klp10A might be able to attack the MT ends and depolymerize long MTs to short filaments. Short MTs were proposed to re-orient randomly and serve as seeds for polymerization [65], potentially resulting in a mixed MT polarity in dendrites.

Consistently, an accompanying paper by the Rumpf laboratory also reports the roles of PP2A in regulating Mical expression and dendrite pruning in the same neurons [45]. In addition to its important role in dendritic MT orientation in our study, their study, however, highlights another critical role of PP2A in regulating the actin dynamics in the dendrites [45]. F-actin undergoes disassembly at the proximal dendrites of ddaC neurons at the onset of dendrite pruning [17]. Since Mical can directly disassemble F-actin via its N-terminal flavoprotein monooxygenase (FM) domain *in vitro* and in bristles [44], it is an excellent candidate for promoting F-actin disassembly during dendrite pruning. Taken together, these two studies provide complementary insights into PP2A functions in regulating both microtubule orientation and actin dynamics during dendrite pruning.

In summary, we have demonstrated a vital role of PP2A in governing dendrite pruning. Mechanistically, PP2A, via two regulatory subunits, Wdb and Tws, regulates the activation of ecdysone signaling as well as the minus-end-out MT orientation in dendrites.

Materials and Methods

Fly strains

UAS-mical and *UAS-mical^{NT}* [66], *SOP-flp (#42)* [67], *ppk-Gal4* on II and III chromosome [68], *UAS-Kin-β-gal* [46], *UAS-EB1-GFP* [69], *UAS-mts-dn* [36], *mts^{299}* [38], *pp2a-29b^{rs}* [38], *tws^{60}* [35], *tws^{603}* (Yu lab), *mical-β-gal* [16], *wdb^{dw}*, and *wdb^{14}* [36].

The following stocks were obtained from Bloomington Stock Centre (BSC): *UAS-mCD8*::GFP, *FRT40A, FRT82B, UAS-Dicer2, Gal4$^{4\text{-}77}$* (BL#8737), *UAS-Nod-β-gal* (BL#9912), *mts* RNAi #1 (BL27723), *pp2a-29b* RNAi #3 (BL#29384), *wdb* RNAi #2 (BL#28939), *wrd* RNAi #1 (BL#38900), *mts^{xe2258}* (BL5684), *klp10a* RNAi # 2 (BL#33963), *tubP-Gal80*, *Gal4$^{109(2)80}$*, *elav-Gal4^{C155}* (BL#458), and UAS-LifeAct-RFP (BL#58362).

The following stocks were obtained from the Vienna *Drosophila* RNAi Centre (VDRC): *mts* RNAi #2 (v41924), *pp2a-29b* RNAi #1 (v49671), *pp2a-29b* RNAi #2 (v49672), *wdb* RNAi #1 (v101406), *tws* RNAi #1 (v34340), *tws* RNAi #2 (v104167), *wrd* RNAi #2 (V22614), *wrd* RNAi #3 (V107057), *pr72* RNAi #1 (V34894), *pr72* RNAi #2 (V107621), *klp10a* RNAi #1 (v41534), *mical* RNAi (V46096), and control RNAi (v36355, v37288).

Immunohistochemistry and antibodies

The following primary antibodies were used for immunohistochemistry at the indicated dilution: mouse anti-β-galactosidase (Promega, 1:1,000), rabbit anti-Klp10A (1:1,000, a gift from D. J. Sharp), mouse anti-EcR-B1 (1:50; AD4.4, DSHB), mouse polyclonal anti-Sox14 (1:200; F. Yu), rabbit anti-Mical (1:200; a gift from A. L. Kolodkin), Guinea pig anti-Msps (1:500; a gift from H. Wang), rabbit anti-TACC (1:500; a gift from J.W.Raff and H.Wang), mouse anti-Patronin (1:250; F. Yu), Phalloidin (Thermo Fisher; 1:100), Cy3 or Cy5-conjugated secondary antibodies (1:500; Jackson Laboratories, Cat#: 111-165-003, 112-095-003). For immunostaining, pupae or larvae were dissected in cold PBS and fixed with 4% formaldehyde for 15 min. Mounting was performed in VECTASHIELD mounting medium, and the samples were directly visualized by the confocal microscopy Leica TSC SP2.

Live imaging of EB1-GFP comet

Larvae at 96 h AEL were immersed with a drop of halocarbon oil (Santa Cruz, Cat#sc-250077) and mounted to slides for confocal imaging. Time-lapse imaging for EB1-GFP comets was recorded with Olympus FV3000 using 60× oil lens with 3× zoom. Eighty-three frames were acquired at 2.25-s intervals with 6 Z-steps. Kymographs were generated for Z-projected time-lapse images using KymographBuilder plugin in Image J.

Live imaging analysis

To image *Drosophila* da neurons, larvae at the wandering 3rd instar (wL3) or pupae at WP stage were first washed in PBS buffer briefly and followed by immersion with 90% glycerol. For imaging da neurons, pupal cases at 16 h APF or 19 h APF were carefully removed before mounted with 90% glycerol. Dendrite images were recorded with Leica TSC SP2.

MARCM analysis of da sensory neurons

MARCM analysis, dendrite imaging, and quantification were carried out as previously described [14]. ddaC clones were chosen and imaged according to their location and morphology at the WP stage. ddaC neurons were examined for dendrite pruning defects at 16 h APF.

RU486/mifepristone treatment for the GeneSwitch system

RU486/mifepristone treatment for the GeneSwitch system was performed as previously described [70]. Embryos were collected at 6 h intervals and reared on standard food to the early 3rd instar larva stage. Subsequently, the larvae grew in the standard culture medium with 240 μg/ml mifepristone (Sigma Aldrich M8046). White prepupae were picked and subjected to phenotypic analysis at WP and/or 16 h APF.

Quantification of ddaC dendrites

Live confocal images of ddaC neurons expressing UAS-mCD8-GFP driven by *ppk-Gal4* were performed at WP, 16 h APF stage. Dorsal is up in all images. The severing defect was defined by the presence of dendrites that remain attached to the soma at 16 h APF. The severing defect in wild-type or mutant ddaC neurons was quantified

in a 275 × 275 μm region of the dorsal dendritic field, originating from the abdominal segments 2–5. The percentage of severing defects is the percentage of ddaC neurons with larval dendrites attached to the soma at 16 h APF. The average number of primary and secondary dendrites attached to soma was computed from wild-type or mutant ddaC neurons. The number of neurons (n) examined in each group is shown on the bars. Sholl analyses of dendrite morphogenesis were conducted using ImageJ. Plots of average length, number of intersections, and SEM were generated using GraphPad Prism software.

Quantification of immunostaining

Images were acquired from projected *z*-stacks (at 1.5 μm intervals) to cover the entire volume of ddaC/D/E sensory neurons using the confocal microscopy Leica TSC SP2. To quantify the fluorescence intensities, cell nuclei (EcR-B1/Sox14 immunostaining) or whole soma (Mical/Klp10A/Patronin/Msps/TACC immunostaining) contours were drawn on the appropriate fluorescent channel based on the GFP channel or relative cellular position in ImageJ software. After subtracting the background (Rolling Ball Radius = 30) on the entire image of that channel, we measured the mean gray value in the marked area in ddaC and ddaE on the same images and calculated their ratios. The ratios were normalized to the corresponding average control values and subjected to statistical analysis for comparison between different conditions. Graphs display the average values of the ddaC/ddaE ratios and the standard error of the mean (SEM) normalized to controls. The number of ddaC neurons (n) examined in each group is shown on the bars. Insets show the ddaC neurons labeled by *ppk-Gal4*-driven *UAS-mCD8-GFP* expression.

To quantify the alterations of dendritic Nod-β-gal distribution, we measured its intensity in the 20 μm of major dorsal dendrites which were 30 μm away from the soma. The number of ddaC neurons (n) examined in each group is shown on the bars. Dorsal is up in all images.

Statistics

For pairwise comparison, two-tailed Student's *t*-test was applied to determine statistical significance. One-way ANOVA with Bonferroni test was applied to determine significance when multiple groups were present. Error bars in all graphs represent SEM. Statistical significance was defined as $***P < 0.001$, $**P < 0.01$, $*P < 0.05$, n.s., not significant. The number of neurons (n) in each group is shown on the bars.

Expanded View for this article is available online.

Acknowledgements

We thank S. Eaton, Y. Jan, A. L. Kolodkin, J.W. Raff, S. Rogers, M.M. Rolls, D.J. Sharp, T. Uemura, H. Wang, the Bloomington Stock Center (BSC), DSHB (University of Iowa), Kyoto Stock Center (Japan), and VDRC (Austria) for generously providing antibodies and fly stocks. We would like to thank S. Rumpf for communicating the results prior to publication. We thank the Yu lab members for helpful discussion. This work was supported by Temasek Life Sciences Laboratory (TLL) Singapore (TLL-2040) and National Research Foundation Singapore (NRF) (SBP-P3 and SBP-P8) (F.Y.).

Author contributions

FY, KSN, and MR conceived and designed the study. KSN and MR performed most of the experiments. QT conducted some Nod-lacZ and Kin-lacZ experiments. SB repeated some EB1-GFP experiments. KSN, MR, and FY analyzed the data. FY and MR wrote the paper.

Conflict of interest

The authors declare that they have no conflict of interest.

References

1. Luo L, O'Leary DD (2005) Axon retraction and degeneration in development and disease. *Annu Rev Neurosci* 28: 127 – 156
2. O'Leary DD, Koester SE (1993) Development of projection neuron types, axon pathways, and patterned connections of the mammalian cortex. *Neuron* 10: 991 – 1006
3. Truman JW (1990) Metamorphosis of the central nervous system of *Drosophila*. *J Neurobiol* 21: 1072 – 1084
4. Lichtman JW, Colman H (2000) Synapse elimination and indelible memory. *Neuron* 25: 269 – 278
5. Kanamori T, Togashi K, Koizumi H, Emoto K (2015) Dendritic remodeling: lessons from invertebrate model systems. *Int Rev Cell Mol Biol* 318: 1 – 25
6. Yu F, Schuldiner O (2014) Axon and dendrite pruning in *Drosophila*. *Curr Opin Neurobiol* 27: 192 – 198
7. Schubiger M, Wade AA, Carney GE, Truman JW, Bender M (1998) *Drosophila* EcR-B ecdysone receptor isoforms are required for larval molting and for neuron remodeling during metamorphosis. *Development* 125: 2053 – 2062
8. Lee T, Marticke S, Sung C, Robinow S, Luo L (2000) Cell-autonomous requirement of the USP/EcR-B ecdysone receptor for mushroom body neuronal remodeling in *Drosophila*. *Neuron* 28: 807 – 818
9. Kuo CT, Jan LY, Jan YN (2005) Dendrite-specific remodeling of *Drosophila* sensory neurons requires matrix metalloproteases, ubiquitin-proteasome, and ecdysone signaling. *Proc Natl Acad Sci USA* 102: 15230 – 15235
10. Williams DW, Truman JW (2005) Cellular mechanisms of dendrite pruning in *Drosophila*: insights from *in vivo* time-lapse of remodeling dendritic arborizing sensory neurons. *Development* 132: 3631 – 3642
11. Selemon LD, Zecevic N (2015) Schizophrenia: a tale of two critical periods for prefrontal cortical development. *Transl Psychiatry* 5: e623
12. Tang G, Gudsnuk K, Kuo SH, Cotrina ML, Rosoklija G, Sosunov A, Sonders MS, Kanter E, Castagna C, Yamamoto A *et al* (2014) Loss of mTOR-dependent macroautophagy causes autistic-like synaptic pruning deficits. *Neuron* 83: 1131 – 1143
13. Han C, Song Y, Xiao H, Wang D, Franc NC, Jan LY, Jan YN (2014) Epidermal cells are the primary phagocytes in the fragmentation and clearance of degenerating dendrites in *Drosophila*. *Neuron* 81: 544 – 560
14. Kirilly D, Gu Y, Huang Y, Wu Z, Bashirullah A, Low BC, Kolodkin AL, Wang H, Yu F (2009) A genetic pathway composed of Sox14 and Mical governs severing of dendrites during pruning. *Nat Neurosci* 12: 1497 – 1505
15. Kuo CT, Zhu S, Younger S, Jan LY, Jan YN (2006) Identification of E2/E3 ubiquitinating enzymes and caspase activity regulating *Drosophila* sensory neuron dendrite pruning. *Neuron* 51: 283 – 290
16. Wong JJ, Li S, Lim EK, Wang Y, Wang C, Zhang H, Kirilly D, Wu C, Liou YC, Wang H *et al* (2013) A Cullin1-based SCF E3 ubiquitin ligase targets the InR/PI3K/TOR pathway to regulate neuronal pruning. *PLoS Biol* 11: e1001657

17. Lee HH, Jan LY, Jan YN (2009) *Drosophila* IKK-related kinase Ik2 and Katanin p60-like 1 regulate dendrite pruning of sensory neuron during metamorphosis. *Proc Natl Acad Sci USA* 106: 6363 – 6368
18. Lin T, Pan PY, Lai YT, Chiang KW, Hsieh HL, Wu YP, Ke JM, Lee MC, Liao SS, Shih HT *et al* (2015) Spindle-F is the central mediator of Ik2 kinase-dependent dendrite pruning in *Drosophila* sensory neurons. *PLoS Genet* 11: e1005642
19. Williams DW, Kondo S, Krzyzanowska A, Hiromi Y, Truman JW (2006) Local caspase activity directs engulfment of dendrites during pruning. *Nat Neurosci* 9: 1234 – 1236
20. Loncle N, Williams DW (2012) An interaction screen identifies headcase as a regulator of large-scale pruning. *J Neurosci* 32: 17086 – 17096
21. Herzmann S, Gotzelmann I, Reekers LF, Rumpf S (2018) Spatial regulation of microtubule disruption during dendrite pruning in *Drosophila*. *Development* 145: dev156950
22. Herzmann S, Krumkamp R, Rode S, Kintrup C, Rumpf S (2017) PAR-1 promotes microtubule breakdown during dendrite pruning in *Drosophila*. *EMBO J* 36: 1981 – 1991
23. Wang Y, Rui M, Tang Q, Bu S, Yu F (2019) Patronin governs minus-end-out orientation of dendritic microtubules to promote dendrite pruning in *Drosophila*. *Elife* 8: e39964
24. Kanamori T, Kanai MI, Dairyo Y, Yasunaga K, Morikawa RK, Emoto K (2013) Compartmentalized calcium transients trigger dendrite pruning in *Drosophila* sensory neurons. *Science* 340: 1475 – 1478
25. Kanamori T, Yoshino J, Yasunaga K, Dairyo Y, Emoto K (2015) Local endocytosis triggers dendritic thinning and pruning in *Drosophila* sensory neurons. *Nat Commun* 6: 6515
26. Zhang H, Wang Y, Wong JJ, Lim KL, Liou YC, Wang H, Yu F (2014) Endocytic pathways downregulate the L1-type cell adhesion molecule neuroglian to promote dendrite pruning in *Drosophila*. *Dev Cell* 30: 463 – 478
27. Loncle N, Agromayor M, Martin-Serrano J, Williams DW (2015) An ESCRT module is required for neuron pruning. *Sci Rep* 5: 8461
28. Zhu S, Chen R, Soba P, Jan YN (2019) JNK signaling coordinates with ecdysone signaling to promote pruning of *Drosophila* sensory neuron dendrites. *Development* 146: dev163592
29. Feng C, Thyagarajan P, Shorey M, Seebold DY, Weiner AT, Albertson RM, Rao KS, Sagasti A, Goetschius DJ, Rolls MM (2019) Patronin-mediated minus end growth is required for dendritic microtubule polarity. *J Cell Biol* 218: 2309 – 2328
30. Janssens V, Longin S, Goris J (2008) PP2A holoenzyme assembly: in cauda venenum (the sting is in the tail). *Trends Biochem Sci* 33: 113 – 121
31. Janssens V, Goris J (2001) Protein phosphatase 2A: a highly regulated family of serine/threonine phosphatases implicated in cell growth and signalling. *Biochem J* 353: 417 – 439
32. Santoro MF, Annand RR, Robertson MM, Peng YW, Brady MJ, Mankovich JA, Hackett MC, Ghayur T, Walter G, Wong WW *et al* (1998) Regulation of protein phosphatase 2A activity by caspase-3 during apoptosis. *J Biol Chem* 273: 13119 – 13128
33. Turowski P, Fernandez A, Favre B, Lamb NJ, Hemmings BA (1995) Differential methylation and altered conformation of cytoplasmic and nuclear forms of protein phosphatase 2A during cell cycle progression. *J Cell Biol* 129: 397 – 410
34. Kiely PA, O'Gorman D, Luong K, Ron D, O'Connor R (2006) Insulin-like growth factor I controls a mutually exclusive association of RACK1 with protein phosphatase 2A and beta1 integrin to promote cell migration. *Mol Cell Biol* 26: 4041 – 4051
35. Uemura T, Shiomi K, Togashi S, Takeichi M (1993) Mutation of twins encoding a regulator of protein phosphatase 2A leads to pattern duplication in *Drosophila* imaginal discs. *Genes Dev* 7: 429 – 440
36. Hannus M, Feiguin F, Heisenberg CP, Eaton S (2002) Planar cell polarization requires Widerborst, a B' regulatory subunit of protein phosphatase 2A. *Development* 129: 3493 – 3503
37. Ogawa H, Ohta N, Moon W, Matsuzaki F (2009) Protein phosphatase 2A negatively regulates aPKC signaling by modulating phosphorylation of Par-6 in *Drosophila* neuroblast asymmetric divisions. *J Cell Sci* 122: 3242 – 3249
38. Wang C, Chang KC, Somers G, Virshup D, Ang BT, Tang C, Yu F, Wang H (2009) Protein phosphatase 2A regulates self-renewal of *Drosophila* neural stem cells. *Development* 136: 2287 – 2296
39. Viquez NM, Li CR, Wairkar YP, DiAntonio A (2006) The B' protein phosphatase 2A regulatory subunit well-rounded regulates synaptic growth and cytoskeletal stability at the *Drosophila* neuromuscular junction. *J Neurosci* 26: 9293 – 9303
40. Snaith HA, Armstrong CG, Guo Y, Kaiser K, Cohen PT (1996) Deficiency of protein phosphatase 2A uncouples the nuclear and centrosome cycles and prevents attachment of microtubules to the kinetochore in *Drosophila* microtubule star (mts) embryos. *J Cell Sci* 109(Pt 13): 3001 – 3012
41. Wassarman DA, Solomon NM, Chang HC, Karim FD, Therrien M, Rubin GM (1996) Protein phosphatase 2A positively and negatively regulates Ras1-mediated photoreceptor development in *Drosophila*. *Genes Dev* 10: 272 – 278
42. Osterwalder T, Yoon KS, White BH, Keshishian H (2001) A conditional tissue-specific transgene expression system using inducible GAL4. *Proc Natl Acad Sci USA* 98: 12596 – 12601
43. Xu Y, Xing Y, Chen Y, Chao Y, Lin Z, Fan E, Yu JW, Strack S, Jeffrey PD, Shi Y (2006) Structure of the protein phosphatase 2A holoenzyme. *Cell* 127: 1239 – 1251
44. Hung RJ, Yazdani U, Yoon J, Wu H, Yang T, Gupta N, Huang Z, van Berkel WJ, Terman JR (2010) Mical links semaphorins to F-actin disassembly. *Nature* 463: 823 – 827
45. Neele W, Ulrike G, Sebastian R (2020) PP2A phosphatase is required for dendrite pruning via actin regulation in *Drosophila*. *EMBO Rep* 21: e48870
46. Clark IE, Jan LY, Jan YN (1997) Reciprocal localization of Nod and kinesin fusion proteins indicates microtubule polarity in the *Drosophila* oocyte, epithelium, neuron and muscle. *Development* 124: 461 – 470
47. Zheng Y, Wildonger J, Ye B, Zhang Y, Kita A, Younger SH, Zimmerman S, Jan LY, Jan YN (2008) Dynein is required for polarized dendritic transport and uniform microtubule orientation in axons. *Nat Cell Biol* 10: 1172 – 1180
48. Satoh D, Sato D, Tsuyama T, Saito M, Ohkura H, Rolls MM, Ishikawa F, Uemura T (2008) Spatial control of branching within dendritic arbors by dynein-dependent transport of Rab5-endosomes. *Nat Cell Biol* 10: 1164 – 1171
49. Rolls MM, Satoh D, Clyne PJ, Henner AL, Uemura T, Doe CQ (2007) Polarity and intracellular compartmentalization of *Drosophila* neurons. *Neural Dev* 2: 7
50. Stepanova T, Slemmer J, Hoogenraad CC, Lansbergen G, Dortland B, De Zeeuw CI, Grosveld F, van Cappellen G, Akhmanova A, Galjart N (2003) Visualization of microtubule growth in cultured neurons via the use of EB3-GFP (end-binding protein 3-green fluorescent protein). *J Neurosci* 23: 2655 – 2664
51. Vaughan KT (2005) TIP maker and TIP marker; EB1 as a master controller of microtubule plus ends. *J Cell Biol* 171: 197 – 200

52. Mattie FJ, Stackpole MM, Stone MC, Clippard JR, Rudnick DA, Qiu Y, Tao J, Allender DL, Parmar M, Rolls MM (2010) Directed microtubule growth, +TIPs, and kinesin-2 are required for uniform microtubule polarity in dendrites. *Curr Biol* 20: 2169 – 2177
53. Nguyen MM, McCracken CJ, Milner ES, Goetschius DJ, Weiner AT, Long MK, Michael NL, Munro S, Rolls MM (2014) Gamma-tubulin controls neuronal microtubule polarity independently of Golgi outposts. *Mol Biol Cell* 25: 2039 – 2050
54. Riccomagno MM, Kolodkin AL (2015) Sculpting neural circuits by axon and dendrite pruning. *Annu Rev Cell Dev Biol* 31: 779 – 805
55. Martin L, Latypova X, Wilson CM, Magnaudeix A, Perrin ML, Terro F (2013) Tau protein phosphatases in Alzheimer's disease: the leading role of PP2A. *Ageing Res Rev* 12: 39 – 49
56. Du TT, Chen YC, Lu YQ, Meng FG, Yang H, Zhang JG (2018) Subthalamic nucleus deep brain stimulation protects neurons by activating autophagy via PP2A inactivation in a rat model of Parkinson's disease. *Exp Neurol* 306: 232 – 242
57. Boulanger A, Clouet-Redt C, Farge M, Flandre A, Guignard T, Fernando C, Juge F, Dura JM (2011) ftz-f1 and Hr39 opposing roles on EcR expression during *Drosophila* mushroom body neuron remodeling. *Nat Neurosci* 14: 37 – 44
58. Schuldiner O, Berdnik D, Levy JM, Wu JS, Luginbuhl D, Gontang AC, Luo L (2008) piggyBac-based mosaic screen identifies a postmitotic function for cohesin in regulating developmental axon pruning. *Dev Cell* 14: 227 – 238
59. Zheng X, Wang J, Haerry TE, Wu AY, Martin J, O'Connor MB, Lee CH, Lee T (2003) TGF-beta signaling activates steroid hormone receptor expression during neuronal remodeling in the *Drosophila* brain. *Cell* 112: 303 – 315
60. Liu T, Feng XH (2010) Regulation of TGF-beta signalling by protein phosphatases. *Biochem J* 430: 191 – 198
61. Kitajima TS, Sakuno T, Ishiguro K, Iemura S, Natsume T, Kawashima SA, Watanabe Y (2006) Shugoshin collaborates with protein phosphatase 2A to protect cohesin. *Nature* 441: 46 – 52
62. Stone MC, Nguyen MM, Tao J, Allender DL, Rolls MM (2010) Global up-regulation of microtubule dynamics and polarity reversal during regeneration of an axon from a dendrite. *Mol Biol Cell* 21: 767 – 777
63. Yalgin C, Ebrahimi S, Delandre C, Yoong LF, Akimoto S, Tran H, Amikura R, Spokony R, Torben-Nielsen B, White KP *et al* (2015) Centrosomin represses dendrite branching by orienting microtubule nucleation. *Nat Neurosci* 18: 1437 – 1445
64. Ori-McKenney KM, Jan LY, Jan YN (2012) Golgi outposts shape dendrite morphology by functioning as sites of acentrosomal microtubule nucleation in neurons. *Neuron* 76: 921 – 930
65. del Castillo U, Winding M, Lu W, Gelfand VI (2015) Interplay between kinesin-1 and cortical dynein during axonal outgrowth and microtubule organization in *Drosophila* neurons. *Elife* 4: e10140
66. Terman JR, Mao T, Pasterkamp RJ, Yu HH, Kolodkin AL (2002) MICALs, a family of conserved flavoprotein oxidoreductases, function in plexin-mediated axonal repulsion. *Cell* 109: 887 – 900
67. Matsubara D, Horiuchi SY, Shimono K, Usui T, Uemura T (2011) The seven-pass transmembrane cadherin Flamingo controls dendritic self-avoidance via its binding to a LIM domain protein, Espinas, in *Drosophila* sensory neurons. *Genes Dev* 25: 1982 – 1996
68. Grueber WB, Ye B, Moore AW, Jan LY, Jan YN (2003) Dendrites of distinct classes of *Drosophila* sensory neurons show different capacities for homotypic repulsion. *Curr Biol* 13: 618 – 626
69. Stone MC, Roegiers F, Rolls MM (2008) Microtubules have opposite orientation in axons and dendrites of *Drosophila* neurons. *Mol Biol Cell* 19: 4122 – 4129
70. Wang Y, Zhang H, Shi M, Liou YC, Lu L, Yu F (2017) Sec71 functions as a GEF for the small GTPase Arf1 to govern dendrite pruning of *Drosophila* sensory neurons. *Development* 144: 1851 – 1862